Materials Today Bio 24 (2024) 100901

Contents lists available at ScienceDirect

Materials Today Bio

journal homepage: www.journals.elsevier.com/materials-today-bio

# The transformation of multifunctional bio-patch to hydrogel on skin wounds for efficient scarless wound healing

Xiaozhang Ying [a,b,c,1], Congcong Yu [a,b,***,1], Wentao Yang [a,b], Lin Ye [a,b], Rongtai Sun [a,b], Tianyuan Gu [a,b], Shunwu Fan [a,b,**], Shasha Yao [a,b,*]

[a] Department of Orthopaedic Surgery, Sir Run Run Shaw Hospital School of Medicine, Zhejiang University, Hangzhou, Zhejiang, 310016, China
[b] Key Laboratory of Musculoskeletal System Degeneration and Regeneration, Translational Research of Zhejiang Province, Hangzhou, Zhejiang, 310016, China
[c] Zhejiang Hospital of Integrated Traditional Chinese and Western Medicine, Hangzhou, Zhejiang, 310003, China

ARTICLE INFO

*Keywords:*
Aloin
Bio-patch
Hydrogel
Scarless
Wound healing

ABSTRACT

Hydrogels have been widely used in various biomedical applications, including skin regeneration and tissue repair. However, the capability of certain hydrogels to absorb exudate or blood from surrounding wounds, coupled with the challenge in their long-term storage to prevent bacterial growth, can pose limitations to their efficacy in biological applications. To address these challenges, the development of a multifunctional aloin-arginine-alginate (short for 3A) bio-patch capable of transforming into a hydrogel upon absorbing exudate or blood from neighboring wounds for cutaneous regeneration is proposed. The 3A bio-patch exhibits outstanding features, including an excellent porous structure, swelling properties, and biodegradability. These characteristics allow for the rapid absorption of wound exudates and subsequent transformation into a hydrogel that is suitable for treating skin wounds. Furthermore, the 3A bio-patch exhibits remarkable antibacterial and anti-inflammatory properties, leading to accelerated wound healing and scarless repair *in vivo*. This study presents a novel approach to the development of cutaneous wound dressing materials.

## 1. Introduction

The skin, being the largest organ in the human body, plays a vital role in protecting the body from external threats [1,2]. Common clinical conditions include acute skin damage and skin defects resulting from accidents [3]. It is crucial to promptly repair damaged skin to prevent the risk of wound infection and the formation of chronic wounds, which can have significant health implications for patients [4,5]. Additionally, the formation of pathological scars during the healing process can impose a heavy psychological burden on patients [6]. Therefore, there is a significant focus in the field of trauma on the development of drugs and preparations that can promote wound healing and reduce the formation of pathological scars [7,8]. However, currently, there are limited treatment options available for scarless wound regeneration.

In recent years, several studies have explored the potential role of hydrogels in wound repair, highlighting their unique advantages as drug carriers [9–11]. Hydrogels have the ability to create a moist wound environment, which has been shown to promote efficient wound healing [12,13]. Additionally, hydrogels can facilitate the acceleration of wound healing, making them highly desirable materials for wound treatment [14,15]. However, despite their numerous benefits, hydrogels possess certain limitations when it comes to practical applications in wound healing. One limitation is their susceptibility to bacterial growth during long-term transportation and use, which can compromise their effectiveness in biological applications [16]. Additionally, some hydrogels have the tendency to absorb excessive exudates or blood from the surrounding wound, potentially diluting or even destroying their structure, thereby impeding the regenerative process [17–19]. Consequently,

* Corresponding author. Department of Orthopaedic Surgery, Sir Run Run Shaw Hospital School of Medicine, Zhejiang University, Hangzhou, Zhejiang, 310016, China.
** Corresponding author. Department of Orthopaedic Surgery, Sir Run Run Shaw Hospital School of Medicine, Zhejiang University, Hangzhou, Zhejiang, 310016, China.
*** Corresponding author. Department of Orthopaedic Surgery, Sir Run Run Shaw Hospital School of Medicine, Zhejiang University, Hangzhou, Zhejiang, 310016, China.
*E-mail addresses:* yucongcong@zju.edu.cn (C. Yu), shunwu_fan@zju.edu.cn (S. Fan), yaoshasha@zju.edu.cn (S. Yao).
[1] These authors contributed equally to this manuscript.

https://doi.org/10.1016/j.mtbio.2023.100901
Received 15 August 2023; Received in revised form 19 November 2023; Accepted 3 December 2023
Available online 9 December 2023

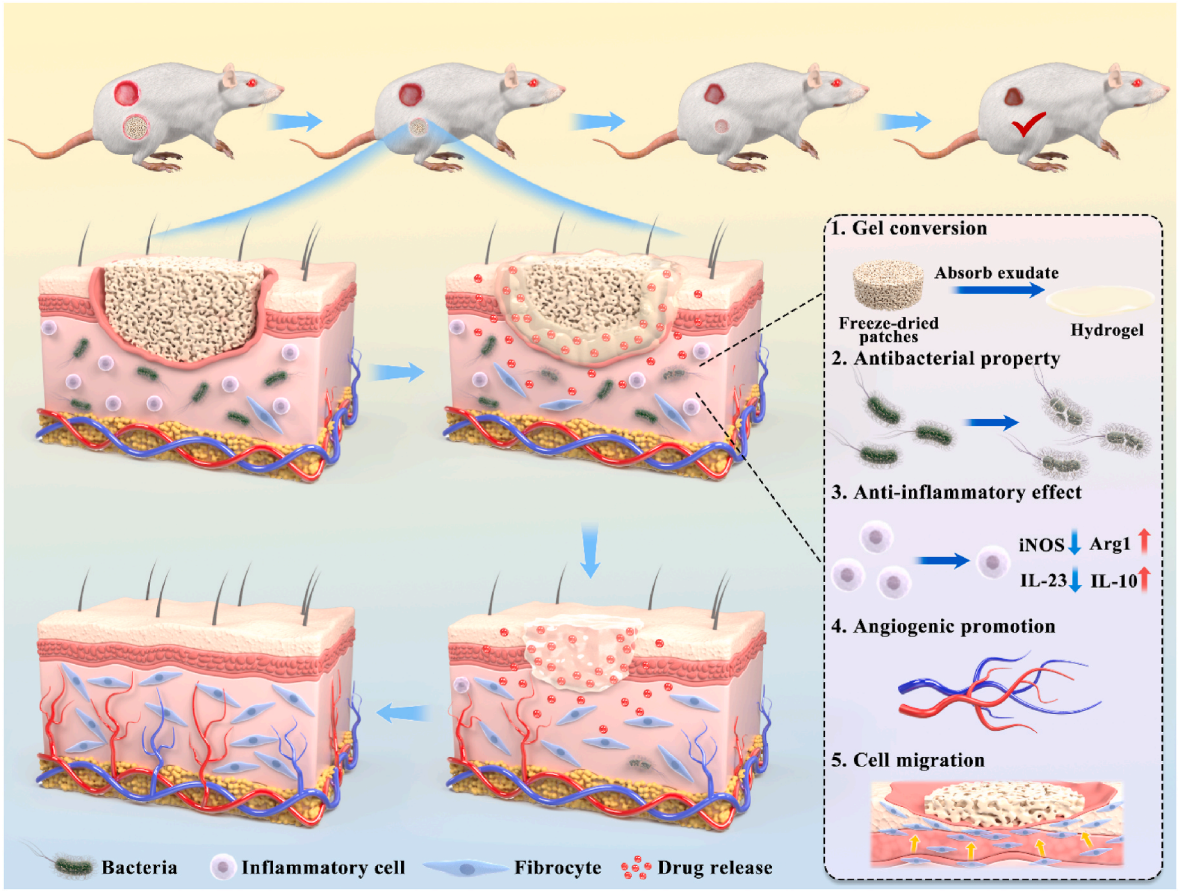


**Scheme 1.** Schematic illustration of the preparation of the 3A bio-patches and the acting process of repairing the infected wound.

there is a pressing need to develop a biological patch that can transform into a hydrogel state upon absorption of exudates from the surrounding wounds, enabling its use in wound regeneration.

Aloe Vera, a plant native to China, has been widely used for its various medicinal properties, particularly in the treatment of skin diseases, since ancient times [20,21]. Aloin, an active ingredient found in Aloe Vera gel, possesses several advantages, such as its simple structure, excellent stability, and superior water solubility [22]. Additionally, studies have reported on the antimicrobial, anti-inflammatory, and anti-cancer properties of aloin [23]. However, limited research has been conducted on the use of aloin to promote wound healing.

Arginine, an amino acid that is conditionally indispensable, has been recommended along with other nutrients to aid in the healing process of wounds [24,25]. It plays a critical role in wound healing by acting as a secretagogue, stimulating the release of growth hormone, and serving as a precursor to nitric oxide (NO), proline, and polyamines [26,27]. The activation of these active nutrients through arginine promotes cell proliferation, enhances angiogenesis, and reduces inflammation [28].

Alginate, known for its high hygroscopicity, glue-forming properties, and hemostatic effects, has been widely used in the treatment of post-operative wounds with bleeding and chronic wounds with high exudate [29,30]. Furthermore, sodium alginate has been found to adsorb bacteria, preventing their entry into the wound, and activate macrophages to defend against the invasion of pathogenic microorganisms [31,32]. In order to optimize the practicality of wound dressing materials for clinical use, alginate is often combined with other polymers to develop wound dressings that are resistant to antimicrobial agents [33].

This section describes a novel hydrogel, known as 3A, composed of aloin, arginine, and alginate, which is proposed as a method for achieving scarless wound healing (see Scheme 1). The 3A hydrogel is biocompatible and has been lyophilized to create a porous and pliable bio-patch with sponge-like characteristics, making it suitable for clinical use in the treatment of acute skin injuries. The unique porous structure, swelling properties, and biodegradability of the dressing biomaterials allow them to absorb wound exudate and form hydrogels that cover skin defects. The aloin bio-patches offer multifunctional benefits during the healing process, including antibacterial properties, reduction of inflammation, promotion of angiogenesis, and facilitation of cell migration and differentiation. By implementing this bio-patch therapy, the healing of acute infected skin injuries is expedited, accompanied by significant regeneration of blood vessels, leading to a scar-free recovery. These findings demonstrate that the dressing hydrogel presents a promising new therapeutic strategy for wound healing in cases of infection.

## 2. Materials and methods

### 2.1. Materials

All reagents and solvents, including aloin, arginine, and alginate were purchased from Aladdin (Shanghai, China) and used without further purification unless otherwise specified. Phosphate buffer saline (PBS) was purchased from Servicebio (Wuhan, China). A Live/Dead viability/cytotoxicity assay kit and Cell Counting Kit-8 (CCK-8) solution were purchased from Proteintech (Wuhan, China). Fetal bovine serum (FBS) and Dulbeccos modified Eagle's medium (DMEM) were provided by Gibco (USA).

### 2.2. Synthesis of Aloin-arginine-alginate hydrogels and bio-patches

In a typical procedure, dissolve aloin (40 mg, 20 mg, 10 mg, and 0 mg) and 1 g sodium alginate in 36 mL of PBS, then add 280 mg EDC and

40 mg NHS under magnetic stirring and continue stirring for 30 min. 40 mg arginine (RGD R/Arg) was added to 4 mL of PBS, and then the arginine solution was added slowly to the above solution. The reaction continued for about 8 h. The hydrogels were obtained and divided into four groups according to the concentration of aloin in the solution: 2A group (0 mg/mL); 3A-0.25 group (0.25 mg/mL); 3A-0.5 group (0.5 mg/mL); 3A-1 group (1 mg/mL). The hydrogels were freeze-dried to obtain the bio-patches.

### 2.3. Characterization of the hydrogels

The fracture surfaces of hydrogels were characterized by scanning electron microscopy (SEM; Hitachi SU8010, Japan), and the porosity ratio was calculated via ImageJ software. Attenuated total reflection-Fourier transform infrared spectroscopy (ATR-FTIR; Perkin-Elmer Spectrum 2, US) was used to conduct the compositional characteristics of the hydrogels.

### 2.4. Adhesive properties of the hydrogels

The mice were humanely euthanized, and subsequently, fresh heart and kidney were extracted. To assess the adhesive properties of the hydrogel, the organs were carefully incised, creating open wounds. The cut surfaces were then treated with the hydrogel to effectively seal the incisions. Samples were taken from the incision site of the hydrogel and adhered tissues for observation of the microstructure using SEM.

### 2.5. Rheological and mechanical properties

Hydrogels containing varying proportions of alginate and arginine were synthesized and their rheological properties were evaluated to determine the optimal ratio. The proportions of alginate to arginine were 0.3 g:40 mg, 0.6 g:40 mg, 1 g:40 mg, and 1.5 g:40 mg. In addition, two commercially available hydrogels, referred to as Flamigel (Flen Pharma N.V., Belgium) and Intrasite gel (Smith&Nephew, UK), were purchased and their rheological and mechanical properties were evaluated for comparison with the 3A-1 hydrogel synthesized in this study.

Rheological experiments were conducted using a rotational rheometer (Anton Paar MCR302, Austria) at 25 °C. Dynamic oscillatory frequency sweep measurements were performed with a strain amplitude of 1%. Continuous oscillatory strain amplitude sweep tests were conducted from 1% to 100% at a frequency of 10 rad $s^{-1}$.

### 2.6. Swelling properties and biodegradability

The freeze-dried hydrogels were soaked in a PBS solution at room temperature and weighed at each predetermined time interval. The calculation formula of the swelling ratio was as follows: $(W_t - W_0)/W_0 \times 100\%$, where $W_t$ and $W_0$ were the initial weight of the hydrogel after freeze-drying and the weight after swelling, respectively.

To assess biodegradability *in vitro*, the freeze-dried hydrogels were immersed in simulated body fluids at 37 °C for 7 days, and the medium was refreshed every 2 days. The hydrogels were collected, rinsed, lyophilized, and weighed to calculate the mass remaining rates at each predetermined time interval.

### 2.7. Cell cultures

Human umbilical vein endothelial cells (HUVECs) and mouse embryo fibroblasts NIH3T3 were obtained from the commercial approach and used *in vitro* experiments, which were incubated in DMEM supplemented with 10% FBS. Macrophage RAW267.4 was purchased from Procell Life Science&Technology (China, Wuhan). In the experiments of co-culturing the hydrogels with cells, the hydrogels were freeze-dried, sterilized, ground into powder, and dispersed in the culture medium at a concentration of 1 mg/mL.

### 2.8. Biocompatibility test

Cells were seeded in 96-well plates at a density of 5000 cells per well and cultured with the hydrogels. After 1, 3, and 5 days of incubation, the CCK-8 reagent was mixed with fresh DMEM medium for culturing for 1 h, and cell viability was quantified at 450 nm. Additionally, a Live/Dead kit was employed to assess cell viability, and the fluorescent images were acquired by a fluorescence microscope.

### 2.9. Angiogenesis assay In vitro

HUVECs were seeded in 24-well plates coated with Matrigel (Corning, US). Hydrogels were added to the medium to assess angiogenic ability. The morphology was monitored under a light microscope regularly. After 6 h, the wells were rinsed with PBS three times and then stained with calcein-AM (ProteninTech, China). Vascular tube lengths were quantified by ImageJ Software in three random fields of view.

### 2.10. Wound scratch migration assay

NIH3T3 cells were cultured with hydrogels to sufficient density in 6-well plates. A cell scraper was used to make a horizontal scratch on the cell monolayer, and free cells were washed with PBS. The medium was replaced by DMEM supplemented with 1% FBS. The cell migration status was observed at 0, 12, 24, and 36 h. The degree of closure in the scratch area was calculated to evaluate cell migration ability.

### 2.11. Antibacterial activity evaluation In vitro

The antibacterial activity of 3A hydrogels was evaluated using an inhibition zone assay against *Staphylococcus aureus* (*S. aureus*) with filter papers (6 mm * 1 mm). The preparation of the bacteria was performed as per previously stated protocols [34]. First, the density of *S. aureus* was adjusted to $10^6$ CFU per mL and then bacteria suspension was spread on the agar surface for inoculation. Afterward, the four hydrogels were placed on the agar plates and co-cultured with *S. aureus* for 24 h at 37 °C. The areas of the bacteriostatic ring were recorded with a camera, and measured by ImageJ software. The inhibition zone was measured by subtracting the diameter of each hydrogel from the diameter of the total inhibition zone.

### 2.12. Hemolysis assay

Fresh anticoagulated mice blood was collected. The hydrogels were added to the blood and incubated for 1 h at 37 °C. The solution was centrifuged to pellet the intact red blood cells, and the absorbance of the supernatant at 545 nm was detected. A distilled water group was set as the positive group, and the hemolysis was calculated accordingly.

### 2.13. Angiogenesis-, skin regeneration-, and inflammation-related gene expressions

HUVECs were cultured with the materials for 3 days, and mRNA was extracted to detect the expression levels of angiogenesis-related genes and collagen markers, including CD31, vascular endothelial growth factor A (VEGFA), collagen type 1 (Col1), and collagen type 3 (Col3). NIH3T3 cells were cultured with the materials for 3 days, and mRNA was extracted to detect the expression levels of skin regeneration-related genes, including fibroblast growth factor 2 (FGF-2) and transforming growth factor beta 1 (TGF-β1). RAW264.7 cells cultured with the hydrogels for 3 days were determined for the expression levels of inflammation-related genes, including inducible nitric oxide synthase (iNOS), interleukin 23 (IL-23), Arginase 1 (Arg1), and interleukin 10 (IL-10). Primers used in this work were referred to in Table S1.

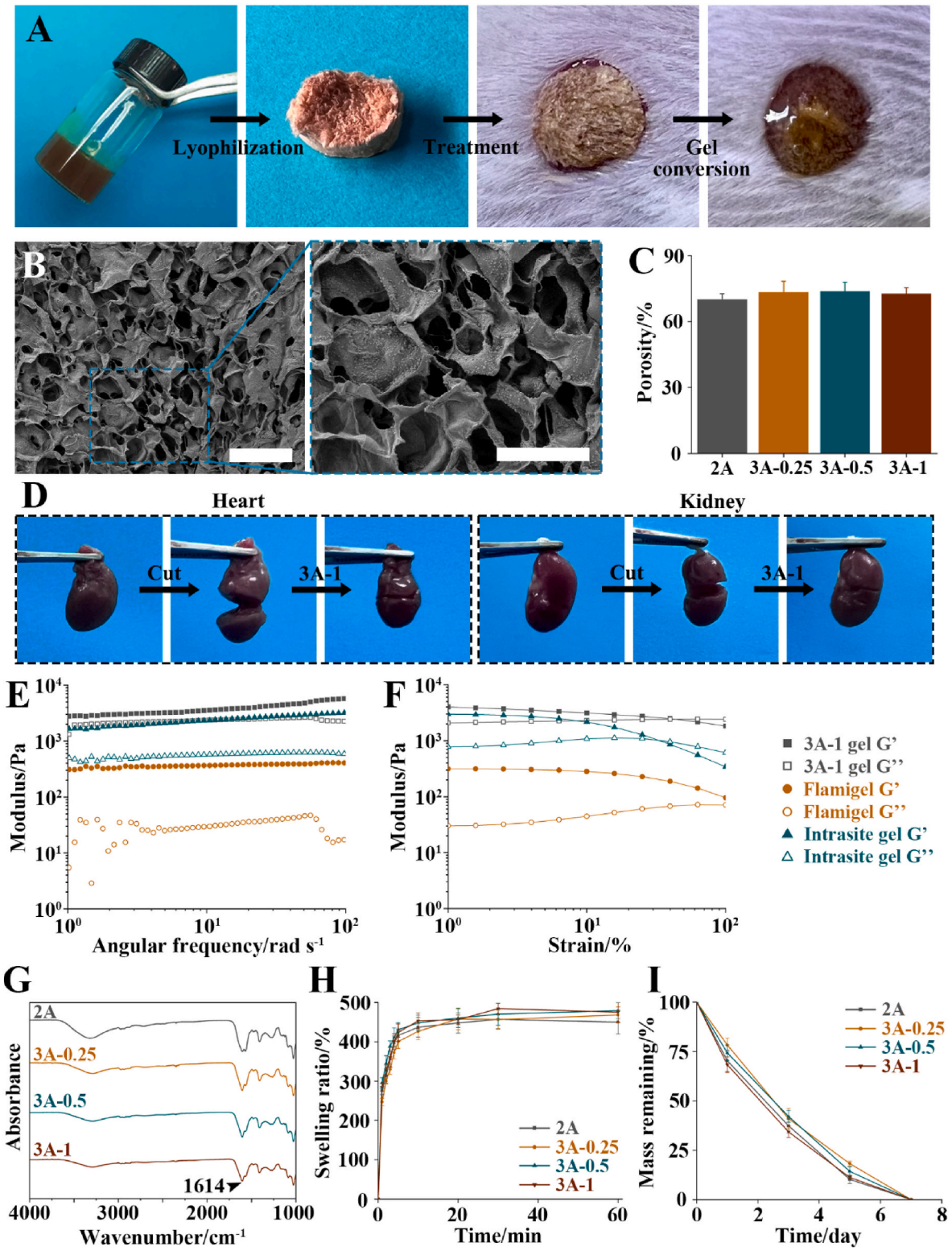


**Fig. 1.** Characterizations of the aloin hydrogel bio-patches. (A) Photographs of the 3A-1 hydrogel and freeze-dried bio-patch. (B) The SEM image of the 3A-1 hydrogel. (C) The porosity rates of the hydrogels (mean ± s.d, n = 3). (D) Two pieces cut from mouse heart and kidney adhered to each other by spreading the 3A-1 hydrogel between them. (E–F) Rheological characterizations of the 3A-1 hydrogel and two commercial hydrogels (Flamigel and Intrasite gel), showing the E) frequency-dependent and F) strain-dependent rheology. (G) The ATR-FTIR spectra of the hydrogels. (H) The swelling properties of the hydrogels (mean ± s.d, n = 3). (I) The mass remaining of the hydrogels within 7 days (mean ± s.d, n = 3). Scale bars: 200 μm and 100 μm (B).

### 2.14. In vivo infected wound healing

Briefly, 45 males, 10-week-old mice were chosen for the experiment. All animal experimental protocols were approved by the animal care and use regulations (Sir Run Run Shaw Hospital Affiliated with the Medical College of Zhejiang University) and the experiments were conducted under the control of Zhejiang University's Guidelines for Animal Experimentation. The accreditation number of the laboratory is SYXK(Zhe)2017-0006. The defective wounds with the infection on the dorsal side of mice were created to evaluate the hydrogels' antibacterial and healing abilities *in vivo*. The animals were divided into five groups in random following as control, 2A, 3A-0.25, 3A-0.5, and 3A-1 groups.

Primarily, we shaved the fur of the dorsal skin in all mice, and then made two circular full-thickness wounds with the same size the diameter of which is 7 mm penetrating skin. Afterward, the typical Gram-positive Bacterium *S. aureus* was inoculated onto the wounds with equal quantity ($1 \times 10^6$ CFU in 50 μL PBS). The wound site was covered by the freeze-dried hydrogel patches, while the control group received no treatment except covered with sterile gauze. All the above-mentioned operations were under the anesthesia of 2.5% pentobarbital (mg/kg). Furthermore, the macroscopic pictures of the wounds were recorded by a digital camera, and the data were analyzed by the ImageJ software at 0, 4, 8, and 12 days after the operation. The closure rate of the wound in different groups at each time point was calculated by the formula:

$$\text{Healing rate } (\%) = \frac{A_0 - A_t}{A_0} \times 100\%$$

where $A_0$ and $A_t$ are the initial wound area and residual wound area at each time point, respectively.

### 2.15. Histological analysis

The harvested samples were fixed in 4% formalin solution overnight, embedded in paraffin, and sectioned into 5 μm thickness. Hematoxylin and eosin (H&E) and Masson's trichrome (MTC) stainings were used to evaluate the infected wound healing. Immunofluorescence (IF) staining was used to analyze collagen deposition and angiogenesis, including cytokeratin 14 (CK14; ProteinTech, China), vascular endothelial growth factor (VEGF; ProteinTech, China), platelet endothelial cell adhesion molecule-1 (CD31; Proteintech, China), and alpha-smooth muscle actin (α-SMA; Proteintech, China). All images were captured by a fluorescence microscope (Zeiss, Germany).

### 2.16. Statistical analysis

All data in the experiments were reported as means ± standard deviations for at least three specimens. The significance of differences between results was evaluated by the One-Way ANOVA test. Probability values such as $^*P < 0.05$, $^{**}P < 0.01$, and $^{***}P < 0.001$ were considered statistically significant.

## 3. Results and discussion

### 3.1. Fabrication and characterization of the hydrogels

To optimize the structure and function of hydrogels for skin wound regeneration, arginine-alginate hydrogels were prepared with varying amounts of aloin (0 mg/mL, 0.25 mg/mL, 0.5 mg/mL, and 1.0 mg/mL). The hydrogels were synthesized through the mixing and crosslinking of EDC, NHS, arginine, alginate, and aloin. Four different hydrogels were created, named as 2A (0 mg/mL aloin), 3A-0.25 (0.25 mg/mL aloin), 3A-0.5 (0.5 mg/mL aloin), and 3A-1 (1.0 mg/mL aloin). Fig. 1A visually depicts the appearance of the 3A-1 hydrogel, which is dark-yellow in color and forms a sponge-like porous patch after freeze-drying. This bio-patch has the capability to adhere to skin wounds, absorb exudate, and gradually reform into a hydrogel, which typically takes approximately 24 h.

SEM images of the hydrogels, as shown in Fig. 1B and Fig. S1, reveal a porous network structure. The porosity rate of the 3A-1 hydrogel was measured to be 72.56 ± 2.84% (Fig. 1C). The adhesive capability of the 3A-1 hydrogel to various tissues was assessed in Fig. 1D, demonstrating its strong affinity for tightly adhering to both mouse heart and kidney tissues. This ensures that the bio-patches and hydrogels could tightly adhere to the wound. To understand the adhesion of biological tissues and hydrogels, the microstructures between the adhered tissues and hydrogels were observed by SEM (Fig. S2). The porous hydrogels penetrated into the tissue incisions, and adhered to the two slices cut from heart or kidney. Strong adhesion facilitates healing of damaged tissue.

The network structure of the functional hydrogel is mainly composed of alginate and arginine, which contribute to the mechanical properties of the hydrogel. To explore the optimal ratio of alginate to arginine, the rheological properties of the hydrogel were tested (Fig. S3). When the alginate content was insufficient (alginate:arginine = 0.6 g:40 mg or 0.3 g:40 mg), the storage modulus (G′) was lower than the loss modulus (G″), which indicates the fluid characteristics. With the increase of alginate ratio, the G′ increased and was higher than the G″, showing the elastic nature, stable network structure, and higher mechanical rigidity [35]. With the change of frequency, the modulus of the hydrogels (alginate: arginine = 1 g:40 mg or 1.5 g:40 mg) almost remained stable, indicating the stability of the hydrogel network structure. When the ratio of alginate to arginine was higher than 1 g:40 mg, increasing alginate content had limited improvement on mechanical properties and may be detrimental to hydrogel synthesis and degradation. Therefore, the functional hydrogels in this study were synthesized with a ratio of alginate to arginine of 1 g:40 mg.

Comparing the mechanical properties with commercial hydrogels helps to gain a more comprehensive understanding of the advantages of the materials studied in this research. The rheological properties of the aloin hydrogel were investigated, and a comparison was made with two commercially available wound dressing hydrogels (Flamigel and Intrasite gel) to assess their mechanical performance (Fig. 1E–F). In frequency-dependent sweep, the moduli of all three hydrogels experienced minimal changes, while in strain-dependent sweep, the modulus of the 3A-1 hydrogel exhibited greater stability. Both in frequency-dependent sweep and strain-dependent sweep, the G' of the 3A-1 hydrogel was found to be higher than that of the commercial hydrogels, indicating a more stable structure and superior mechanical performance of the aloin hydrogel.

To confirm the formation of the hydrogels, ATR-FTIR analysis was conducted (Fig. 1G). The results indicated the stretching vibration peak of the C–O group at 1036 $cm^{-1}$, corresponding to the carboxyl group of alginate or arginine [36,37]. Furthermore, broad peaks appeared at 3100–3500 $cm^{-1}$, attributed to the hydroxyl group of aloin or alginate [38,39]. The ATR-FTIR spectrum of the 2A hydrogel revealed that the peak at 1604 $cm^{-1}$ corresponded to the carboxylate group of alginate [40]. However, upon the addition of aloin (in the 3A-0.25, 3A-0.5, and 3A-1 hydrogels), this peak shifted to 1614 $cm^{-1}$, indicating the influence of hydrogen bonding formed between aloin and alginate or arginine [41]. These results confirm the interaction of aloin, alginate, and arginine in the hydrogel synthesis process. To ensure that the hydrogel patches effectively absorb wound exudate, the swelling properties of the hydrogels were evaluated. Fig. 1H demonstrates that the multifunctional 3A hydrogel patch rapidly absorbs surrounding fluids in the early stage and reaches swelling equilibrium (453.24 ± 20.30%) within 10 min. This swelling property is attributed to the porous structure of the hydrogel, which facilitates the maintenance of a stable shape and a moist environment on the wound. To evaluate the biodegradability of the hydrogels, the materials were immersed in simulated body fluid. Within 7 days, the hydrogel patches exhibited substantial degradation (Fig. 1I), indicating good biocompatibility and suitability for the repair

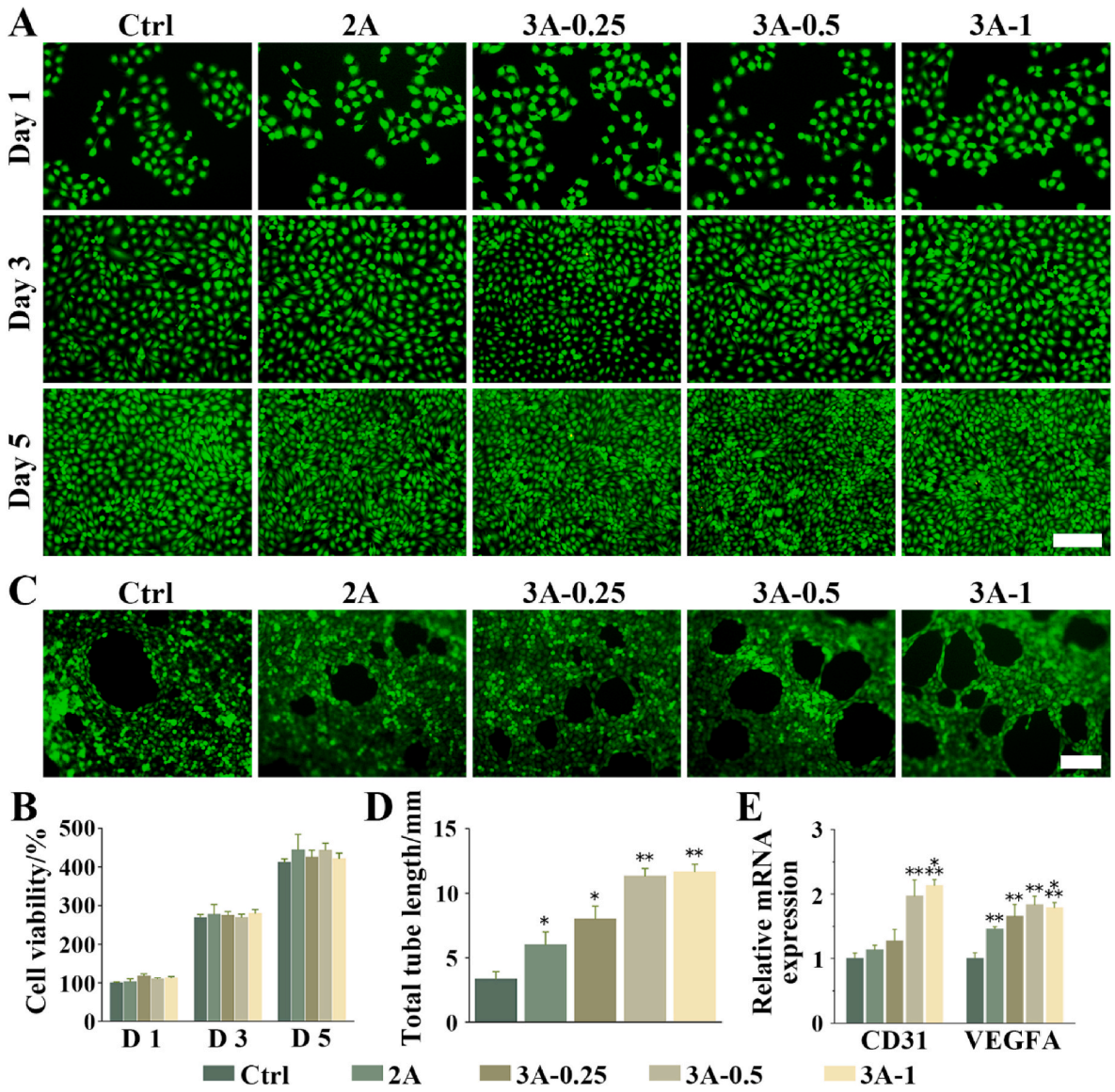


**Fig. 2.** *In vitro* cytocompatibility and angiogenesis capability of the hydrogel bio-patches. (A) Live/Dead staining of HUVECs cultured with the hydrogels for 1, 3, and 5 days. (B) The proliferation of HUVECs culture with the hydrogels (mean ± s.d, n = 3). (C) The tube formation of HUVECs cultured with the hydrogels. (D) Quantitative analysis of total tube length (mean ± s.d, n = 3, *p < 0.05, **p < 0.01). (E) The mRNA expression levels of angiogenesis-related genes, including CD31 and VEGFA (mean ± s.d, n = 3, **p < 0.01, ***p < 0.001). Scale bars: 200 μm (A and C).

cycle of acute skin injuries.

### 3.2. Biocompatibility and angiogenesis assay

The biocompatibility of the hydrogels was assessed using Live/Dead staining and a CCK8 assay over a period of 1, 3, and 5 days of culture. The results, depicted in Fig. 2A–B, revealed no significant differences among the five groups throughout the entire period. After 1 day of incubation, most HUVECs maintained their characteristic spindle-like morphology. At 3 and 5 days, they exhibited robust proliferative activity, indicating favorable biocompatibility of the aloin hydrogel. These findings were further supported by the results of the CCK-8 assay, which showed similar optical density (OD) values in all groups with no significant differences. Moreover, the OD values increased over time, indicating that the cells maintained good vitality and proliferative ability. Together, these results verify that HUVECs maintained their spindle-like morphology, viability, and proliferation, thus confirming the good biocompatibility of the hydrogels. Similarly, NIH3T3 cells also demonstrated excellent proliferative activity when co-cultured with the hydrogels (Fig. S4).

To evaluate the impact of the hydrogels on angiogenesis *in vitro*, tube-formation assays were conducted. An ideal wound dressing should possess both antibacterial properties and the ability to promote angiogenesis. As shown in Fig. 2C, a significant increase in endothelial tube formation was observed in the hydrogel-treated groups compared to the control group. Quantitative analysis revealed that the total tube lengths treated with the 2A, 3A-0.25, 3A-0.5, and 3A-1 hydrogels were 1.80-fold, 2.40-fold, 3.40-fold, and 3.50-fold the length of those in the control group, respectively (Fig. 2D). To assess the effect of the hydrogel on angiogenesis at the molecular level, the mRNA expression levels of genes associated with angiogenesis were measured (Fig. 2E). The 3A-1 hydrogel significantly upregulated the expression of CD31 and VEGFA [42], further confirming the potential of the hydrogels to promote angiogenesis, which may be beneficial for wound healing *in vivo*.

### 3.3. Cytobiological effects and antibacterial property

The effect of the aloin hydrogels on cell migration ability was

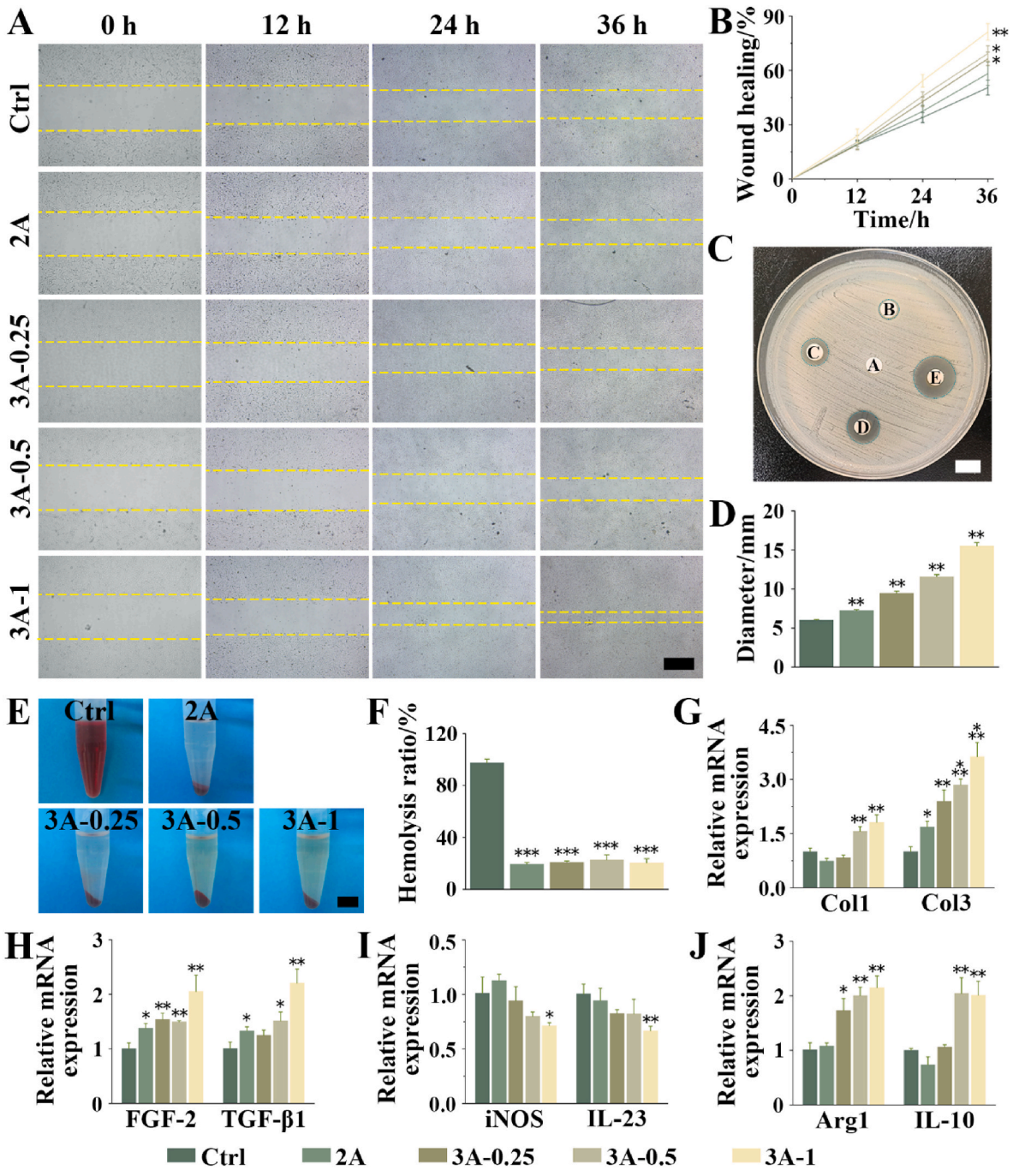


**Fig. 3.** Cytobiological effects and antibacterial properties of the aloin hydrogel bio-patches. (A) Wound scratch migration assay of NIH3T3 cells cultured with the hydrogels. (B) Quantified analysis of wound healing rates (mean ± s.d, n = 3, *p < 0.05, **p < 0.01). (C) Antibacterial sensitivity of the hydrogels against *S. aureus* with agar diffusion test. (D) Inhibition zone diameters for *S. aureus* (mean ± s.d, n = 3, **p < 0.01). (E) Hemolytic test of the hydrogels. (F) Quantitative hemolysis ratio of the hydrogels (mean ± s.d, n = 3, ***p < 0.001). (G) The mRNA expression levels of collagen markers (mean ± s.d, n = 3, *p < 0.05, **p < 0.01, ***p < 0.001). (H) The mRNA expression levels of skin regeneration-related genes, including FGF-2 and TGF-β1 (mean ± s.d, n = 3, *p < 0.05, **p < 0.01). (I) The mRNA expression levels of pro-inflammatory factors, including iNOS and IL-23 (mean ± s.d, n = 3, *p < 0.05, **p < 0.01). (J) The mRNA expression levels of anti-inflammatory factors, including Arg1 and IL-10 (mean ± s.d, n = 3, *p < 0.05, **p < 0.01). Scale bars: 500 μm (A), and 1 cm (C and E).

investigated using a wound scratch migration assay. The 3A-1 group showed a significantly smaller gap remaining compared to the control group (Fig. 3A). Quantitative analysis revealed that the wound healing rate of the 3A-1 group was 1.61 times higher than that of the control group at 36 h (Fig. 3B). These findings suggest that aloin hydrogels significantly improve cell migration ability, which is beneficial for skin repair.

Delayed wound healing is often caused by a weak immune defense and a high risk of bacterial infection [43]. In this study, we focused on the design of anti-bacterial dressings targeting *S. aureus*, the dominant bacteria in wound infections [44]. The anti-S. aureus activities of the prepared hydrogels were evaluated using an agar diffusion assay method. Over 24 h, the diameters of the antibacterial rings gradually increased with increasing aloin concentration. The zone diameters of the 2A, 3A-0.25, 3A-0.5, and 3A-1 groups were measured as 7.23 ± 0.12 mm, 9.46 ± 0.27 mm, 11.57 ± 0.29 mm, and 15.23 ± 0.29 mm,

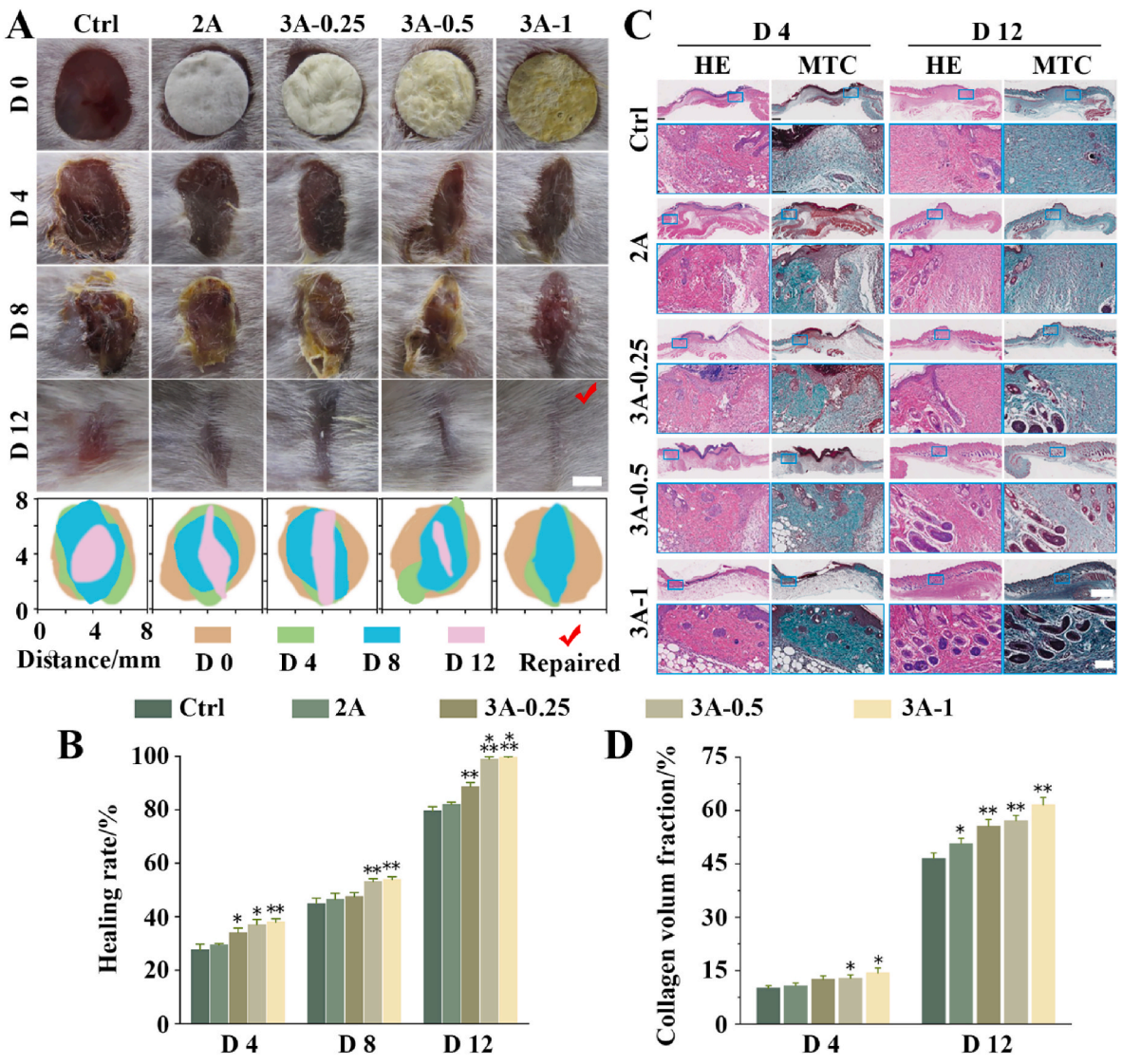


**Fig. 4.** *In vivo* infected wound healing of the aloin bio-patches. (A) Representative images of wound tissues and the area traces of wound closure treated with the hydrogels. (B) Quantification of healing rates (mean ± s.d, n = 3, *p < 0.05, **p < 0.01, ***p < 0.001). (C) Histological analysis of H&E and MTC stained wound tissues. (D) Statistical results of the collagen volume fraction indicated by MTC staining (mean ± s.d, n = 3, *p < 0.05, **p < 0.01). Scale bars: 2 mm (A), 500 μm, and 100 μm (C).

respectively (Fig. 3C–D). These findings indicate that the hydrogels possess effective antibacterial properties through the release of aloin.

Blood compatibility is crucial for the clinical application of biomaterials, and the hemolysis rate is an important factor to consider [45]. Compared to the positive control group, the hydrogel group demonstrated an extremely low hemolysis rate, indicating excellent blood compatibility (Fig. 3E–F).

To further evaluate the cellular biological effects of the hydrogel, the expression levels of multiple genes related to skin regeneration, pro-inflammation, and anti-inflammation were analyzed. Collagen is essential for skin repair and regeneration, as it aids in the repair and reconstruction of damaged tissue [46]. Treatment with aloin hydrogels led to significantly increased expression levels of Col1 and Col3 (Fig. 3G). The expression levels of Col3 in the 2A, 3A-0.25, 3A-0.5, and 3A-1 groups were 1.68-fold, 2.40-fold, 2.85-fold, and 3.63-fold higher than that of the control group, respectively. FGF-2 and TGF-β1 promote the proliferation and migration of various cell types involved in wound healing, as well as stimulate collagen synthesis and remodeling [47]. The multifunctional aloin hydrogels significantly altered the expression levels of these skin regeneration-related genes, particularly in the 3A-1 group, where the expression levels of FGF-2 and TGF-β1 were up-regulated by 1.05 and 1.10 times, respectively (Fig. 3H).

Inhibiting the inflammatory response and associated tissue damage is crucial for accelerating skin repair [48]. The 3A-1 hydrogel significantly inhibited the expression of pro-inflammatory factors (Fig. 3I), while promoting the upregulation of anti-inflammatory factors in the hydrogel-treated groups (Fig. 3J). The expression levels of Arg1 and IL-10 in the 3A-1 group were 2.15-fold and 2.01-fold higher than that of the control group, respectively.

In summary, the aloin hydrogel exhibits diverse cellular functions, including promoting angiogenesis, facilitating cell migration, inhibiting bacteria, promoting skin repair, and controlling inflammation. By harnessing the multifunctional properties of the aloin bio-patches, it is expected to achieve accelerated repair and scar-free healing of infected skin defects *in vivo*.

### 3.4. Evaluation of wound healing and anti-bacterial efficacy In vivo

The effectiveness of wound healing and anti-bacterial properties of different bio-patches (2A, 3A-0.25, 3A-0.5, and 3A-1) was investigated

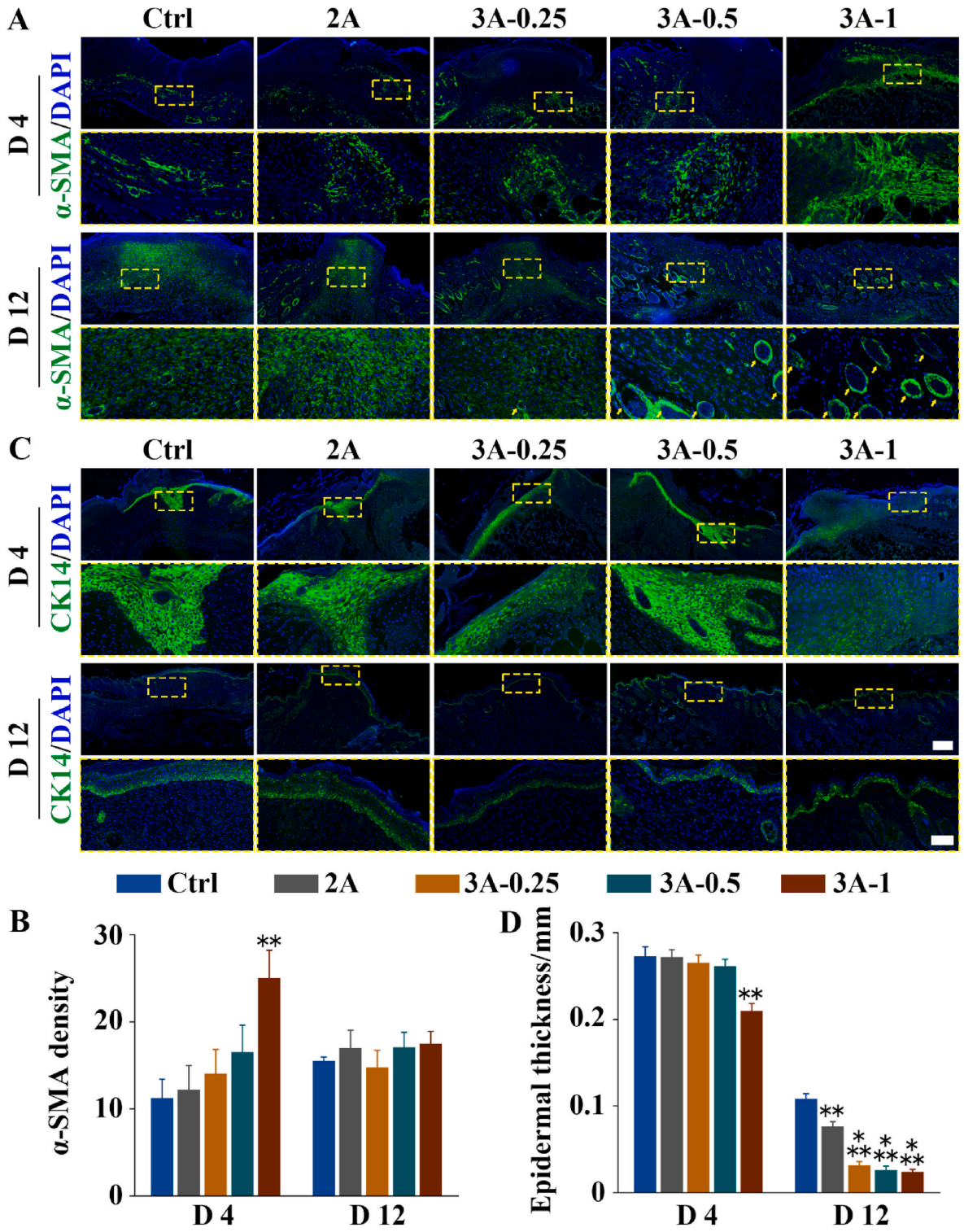


**Fig. 5.** IF staining for α-SMA and CK14. (A) IF staining for α-SMA at 4 and 12 days. The yellow arrows indicating the skin appendages. (B) The quantitative fluorescence density of α-SMA (mean ± s.d, n = 3, **p < 0.01). (C) IF staining of CK14 at 4 and 12 days. (D) The epidermal thickness was measured and quantified from the staining of CK14 (mean ± s.d, n = 3, **p < 0.01, ***p < 0.001). Scale bars: 200 μm and 50 μm (C). (For interpretation of the references to color in this figure legend, the reader is referred to the Web version of this article.)

*in vivo* by creating two full-thickness excisional wounds that were infected with *S. aureus*. The healing progression at different time points is shown in Fig. 4A. In the initial stages of trauma, the control and 2A groups exhibited a significant amount of yellow pus dispersing in the wound bed, while other groups showed minimal presence of yellow pus throughout the entire healing process due to the presence of aloin hydrogels. By day 4, the wounds treated with 3A-1 hydrogel appeared drier and smaller, indicating effective control of infections and initiation of the wound repair process. In the first 8 days, the wound healing area in the control group increased slowly, which could be attributed to the uncontrolled infection. In contrast, the healing rates on day 8 in the 3A-0.5 and 3A-1 hydrogel groups were higher than that in the control group

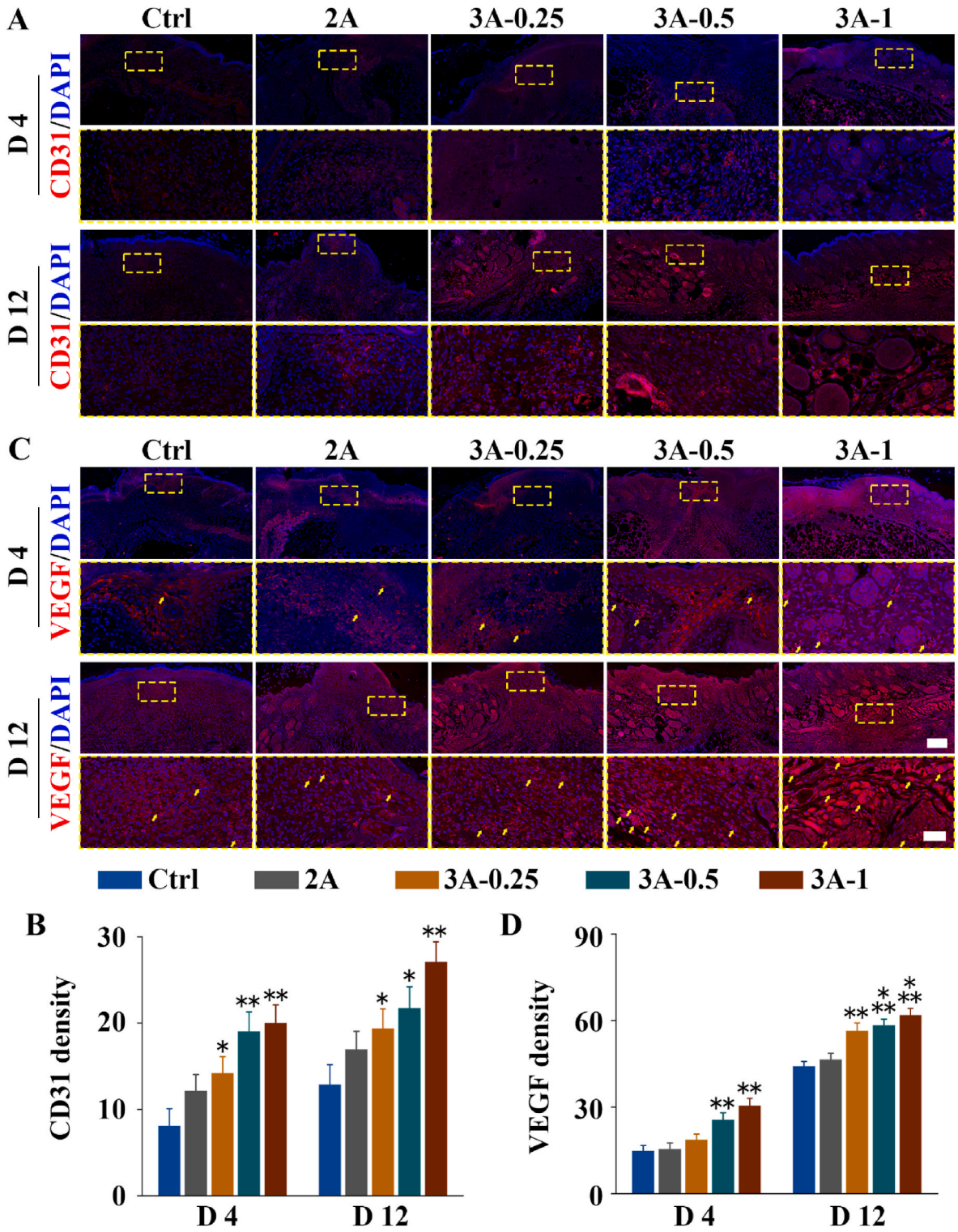


**Fig. 6.** IF staining for CD31 and VEGF. (A) IF staining for CD31 at 4 and 12 days. (B) The quantitative fluorescence density of CD31 (mean ± s.d, n = 3, *p < 0.05, **p < 0.01). (C) IF staining of VEGF at 4 and 12 days. The yellow arrows indicating the blood vessels. (D) The quantitative fluorescence density of VEGF (mean ± s.d, n = 3, **p < 0.01, ***p < 0.001). Scale bars: 200 μm and 50 μm (C). (For interpretation of the references to color in this figure legend, the reader is referred to the Web version of this article.)

(44.93 ± 2.00%), reaching 53.10 ± 1.11% and 53.93 ± 1.01%, respectively, due to the release of aloin and arginine during the early stage. As treatment was prolonged, the wound healing area continued to increase, with the 3A-1 group showing a wound closure rate of 99.67 ± 0.28% on day 12 (Fig. 4B), compared to 81.90 ± 1.01% in the 2A group and 79.53 ± 1.63% in the control group. Macroscopic observations demonstrate that the 3A-1 hydrogel has significant potential to enhance the healing of infected wounds and exhibit antibacterial properties.

Wound samples were collected at each time point and subjected to H&E staining and MTC staining. As shown in Fig. 4C, the control group exhibited almost no epidermis structure after 4 days of treatment, whereas the 3A-1 group clearly showed regenerated epidermis.

Additionally, in the 3A group, the wound gradually presented a volcano-like shape in the first 4 days, primarily due to the newly regenerated tissue around the wound shrinking from the outside towards the center. The size of the wound decreased gradually with increased healing time in all groups. In the 3A-1 group, the defect was almost closed after 12 days of treatment, with numerous hair follicles observed in the healing site, which was similar to normal tissues. However, the control group did not show clear epidermal tissue structure at the same time period, and the defect was still evident with granulation tissue. The volume fractions of collagen fibrils in the repaired epithelial tissue were determined (Fig. 4D). On day 4, the volume fraction of collagen fibrils in the 3A-1 group (14.36 ± 1.37%) was higher than that in the control group (10.09 ± 0.67%) and the 2A group (10.77 ± 0.75%). By day 12, the volume fraction of collagen fibrils had increased in all groups except for the control group, and the 3A-1 group had a collagen volume fraction of 61.60 ± 2.06%. The number of hair follicles increased in the hydrogel-treated groups, particularly in the 3A-1 group. Overall, the multifunctional aloin bio-patches significantly accelerated the proliferation of fibrous connective tissue and the regeneration of skin appendages in the wound.

### 3.5. Histological analysis

To assess the histological healing of the skin, we performed IF staining to detect the expression of keratin and collagen in the repaired sites [49]. The protein α-SMA plays a crucial role in promoting the repair and regeneration of damaged skin tissue [50]. On day 4, we observed abundant α-SMA expression in the newly healed tissues of the 3A-1 group (Fig. 5A). The quantified α-SMA density in this group was 2.22 times higher than that of the control group (Fig. 5B). During the initial phases of skin injury, the healing tissue did not show the presence of skin appendages (sebaceous gland, sweat gland, and hair follicle). Although there was no significant difference in α-SMA expression between all groups at 12 days, the new skin tissues of the 3A-0.5 and 3A-1 groups had more abundant α-SMA-stained skin appendages. In the remaining groups, the formation of thick scar tissues following skin injury impeded the development of skin appendages.

CK14 is predominantly localized in the basal layer of the skin, specifically within the regenerative basal cells [51]. The proliferative scar tissue exhibits pronounced epithelial hypertrophy, and quantitative assessment of the thickness of the CK14-stained renascent epithelium aids in evaluating scar formation [52]. The regeneration of epithelial tissue on day 4 was thickest in all groups, and the thickness of the epithelium tended to become thinner over time (Fig. 5C). On day 12, the prominent scar tissue in the 3A-1 group showed a significant reduction, exhibiting a structure highly similar to normal tissue (Fig. S5). The epithelial thickness of the control, 2A, 3A-0.25, 3A-0.5, and 3A-1 groups was measured as 108.17 ± 6.21, 76.33 ± 5.51, 31.50 ± 4.51, 26.17 ± 4.54, and 24.02 ± 3.01 μm, respectively (Fig. 5D). The skin defects treated with the functional bio-patches achieved scarless healing, closely resembling normal tissue with almost identical epithelial thickness (19.93 ± 2.40 μm).

The formation of new blood vessels plays a vital role in delivering oxygen and nutrients to the site of injury, promoting tissue healing and regeneration [53]. We assessed the vascularization ability by examining the fluorescence expression of vascular endothelial-specific markers, CD31 and VEGF [54,55]. The hydrogel-treated groups showed higher CD31 expression throughout the wound healing cycle (Fig. 6A). On day 12, the quantitative CD31 density of the 2A, 3A-0.25, 3A-0.5, and 3A-1 groups was measured as 1.31-fold, 1.50-fold, 1.69-fold, and 2.10-fold of that in the control group, respectively (Fig. 6B). Similarly, the treatment with aloin bio-patches resulted in increased VEGF expression in the new skin tissues (Fig. 6C–D). VEGF staining amplifies the visibility of blood vessel morphology, making it more distinct. During the initial phases of skin injury, there was limited blood vessel formation, and the morphology appeared disordered. As the wound progressively healed, the application of the aloin bio-patches to the regenerating skin tissue led to a substantial increase in well-structured blood vessel formation, especially in the 3A-0.5 and 3A-1 groups. The multifunctional bio-patches effectively stimulate the growth of blood vessels, thereby expediting the healing process of skin wounds.

Taken together, these findings suggest that the multifunctional aloin bio-patches create an excellent microenvironment platform for reconstructing vascular networks, which may be highly beneficial for improving infected wound healing.

## 4. Conclusions

In this study, we propose the use of a multifunctional aloin bio-patch for the repair and treatment of acutely infected skin defects. The dressing bio-patches are developed through the cross-linking of arginine with aloin using hydrogen bonding. These patches are characterized by their excellent porous structure, swelling properties, and biodegradability. Upon application, the freeze-dried patch absorbs exudates from the wound and adheres to the defects, providing protection while transforming into hydrogels to promote efficient regeneration.

*In vitro* experiments have been conducted to confirm the various biological functions exhibited by the aloin patches. These functions include the promotion of angiogenesis, facilitation of cell migration, inhibition of bacteria, and reduction of inflammation. The multifunctional nature of these patches accelerates the healing of infected wounds and results in scarless repair *in vivo*. Overall, our study presents a new and innovative strategy for the design of cutaneous wound dressing materials. This approach holds promise for the effective treatment of acutely infected skin defects and represents a significant advancement in the field.

## CRediT authorship contribution statement

**Xiaozhang Ying:** Investigation, Methodology, Visualization, Writing - original draft. **Congcong Yu:** Data curation, Investigation, Visualization, Writing - original draft. **Wentao Yang:** Conceptualization, Validation. **Lin Ye:** Methodology, Validation. **Rongtai Sun:** Investigation, Supervision. **Tianyuan Gu:** Methodology. **Shunwu Fan:** Funding acquisition, Supervision, Writing - review & editing. **Shasha Yao:** Conceptualization, Funding acquisition, Methodology, Writing - review & editing.

## Declaration of competing interest

The authors declare that they have no known competing financial interests or personal relationships that could have appeared to influence the work reported in this paper.

## Data availability

Data will be made available on request.

## Acknowledgements

The study was supported by the National Natural Science Foundation of China (Grant No. 82002284), the Health Commission of Zhejiang Province (Grant No. 2021449373), the National Science and Technology Major Project (Grant Nos. 2020YFC1107100).

## Appendix A. Supplementary data

Supplementary data to this article can be found online at https://doi.org/10.1016/j.mtbio.2023.100901.

## References


[1] C. Cao, Z. Xiao, Y. Wu, C. Ge, Diet and skin Aging-from the perspective of food nutrition, Nutrients 12 (3) (2020).
[2] A. Nourian Dehkordi, F. Mirahmadi Babaheydari, M. Chehelgerdi, S. Raeisi Dehkordi, Skin tissue engineering: wound healing based on stem-cell-based therapeutic strategies, Stem Cell Res. Ther. 10 (1) (2019) 111.
[3] K. Raziyeva, Y. Kim, Z. Zharkinbekov, K. Kassymbek, S. Jimi, A. Saparov, Immunology of acute and chronic wound healing, Biomolecules 11 (5) (2021).
[4] S.A. Eming, P. Martin, M. Tomic-Canic, Wound repair and regeneration: mechanisms, signaling, and translation, Sci. Transl. Med. 6 (265) (2014) 265sr6.
[5] W. Peng, D. Li, K. Dai, Y. Wang, P. Song, H. Li, P. Tang, Z. Zhang, Z. Li, Y. Zhou, C. Zhou, Recent progress of collagen, chitosan, alginate and other hydrogels in skin repair and wound dressing applications, Int. J. Biol. Macromol. 208 (2022) 400–408.
[6] M. Monavarian, S. Kader, S. Moeinzadeh, E. Jabbari, Regenerative scar-free skin wound healing, Tissue Eng., Part B 25 (4) (2019) 294–311.
[7] B. Berman, A. Maderal, B. Raphael, Keloids and hypertrophic scars: pathophysiology, classification, and treatment, Dermatol. Surg. 43 (Suppl 1) (2017) S3–s18.
[8] K.C. Hsu, C.W. Luan, Y.W. Tsai, Review of Silicone gel Sheeting and Silicone gel for the prevention of hypertrophic scars and Keloids, Wounds : a compendium of clinical research and practice 29 (5) (2017) 154–158.
[9] A. Mellati, E. Hasanzadeh, M. Gholipourmalekabadi, S.E. Enderami, Injectable nanocomposite hydrogels as an emerging platform for biomedical applications: a review, Mater. Sci. Eng. C Mater. Biol. Appl. 131 (2021), 112489.
[10] L. Qi, C. Zhang, B. Wang, J. Yin, S. Yan, Progress in hydrogels for skin wound repair, Macromol. Biosci. 22 (7) (2022), e2100475.
[11] L.P. da Silva, R.L. Reis, V.M. Correlo, A.P. Marques, Hydrogel-Based strategies to advance Therapies for chronic skin wounds, Annu. Rev. Biomed. Eng. 21 (2019) 145–169.
[12] K. Kaplani, S. Koutsi, V. Armenis, F.G. Skondra, N. Karantzelis, S. Champeris Tsaniras, S. Taraviras, Wound healing related agents: ongoing research and perspectives, Adv. Drug Deliv. Rev. 129 (2018) 242–253.
[13] S.H. Tan, D.A.C. Chua, J.R.J. Tang, C. Bonnard, D. Leavesley, K. Liang, Design of hydrogel-based scaffolds for in vitro three-dimensional human skin model reconstruction, Acta Biomater. 153 (2022) 13–37.
[14] M. Zhang, X. Zhao, Alginate hydrogel dressings for advanced wound management, Int. J. Biol. Macromol. 162 (2020) 1414–1428.
[15] R.C. Op 't Veld, X.F. Walboomers, J.A. Jansen, F. Wagener, Design considerations for hydrogel wound dressings: Strategic and molecular Advances, Tissue Eng., Part B 26 (3) (2020) 230–248.
[16] S. Cascone, G. Lamberti, Hydrogel-based commercial products for biomedical applications: a review, Int. J. Pharm. 573 (2020), 118803.
[17] J. Lan, L. Shi, W. Xiao, X. Zhang, S. Wang, A rapid self-pumping organohydrogel dressing with Hydrophilic fractal Microchannels to promote burn wound healing, Adv. Mater. (2023), e2301765.
[18] J. Lan, L. Shi, W. Xiao, X. Zhang, Y. Wang, S. Wang, An enhanced fractal self-pumping dressing with continuous drainage for accelerated burn wound healing, Front. Bioeng. Biotechnol. 11 (2023), 1188782.
[19] R. Zhang, S. Wang, X. Ma, S. Jiang, T. Chen, Y. Du, M. Cheng, J. Liu, Y. Yuan, T. Ye, S. Wang, In situ gelation strategy based on ferrocene-hyaluronic acid organic copolymer biomaterial for exudate management and multi-modal wound healing, Acta Biomater. 154 (2022) 180–193.
[20] J. Xiao, S. Chen, Y. Chen, J. Su, The potential health benefits of aloin from genus Aloe, Phytother Res. 36 (2) (2022) 873–890.
[21] Y. Yang, J.J. Wu, J. Xia, Y. Wan, J.F. Xu, L. Zhang, D. Liu, L. Chen, F. Tang, H. Ao, C. Peng, Can aloin develop to medicines or healthcare products? Biomed. Pharmacother. 153 (2022), 113421.
[22] M. Kim, J.H. Park, Isolation of aloe saponaria-Derived extracellular vesicles and investigation of their potential for chronic wound healing, Pharmaceutics 14 (9) (2022).
[23] V. De Caro, A.L. Scaturro, G. Di Prima, G. Avellone, F.M. Sutera, O. Di Fede, G. Campisi, L.I. Giannola, Aloin delivery on buccal mucosa: ex vivo studies and design of a new locoregional dosing system, Drug Dev. Ind. Pharm. 41 (9) (2015) 1541–1547.
[24] F. Reesi, M. Minaiyan, A. Taheri, A novel lignin-based nanofibrous dressing containing arginine for wound-healing applications, Drug Deliv. Transl. Res. 8 (1) (2018) 111–122.
[25] Y. Hussein, E.M. El-Fakharany, E.A. Kamoun, S.A. Loutfy, R. Amin, T.H. Taha, S. A. Salim, M. Amer, Electrospun PVA/hyaluronic acid/L-arginine nanofibers for wound healing applications: nanofibers optimization and in vitro bioevaluation, Int. J. Biol. Macromol. 164 (2020) 667–676.
[26] J.K. Stechmiller, B. Childress, L. Cowan, Arginine supplementation and wound healing, Nutr. Clin. Pract. 20 (1) (2005) 52–61.
[27] C.C. Wang, T.Y. Shih, Y.T. Hsieh, J.L. Huang, J. Wang, l-Arginine Grafted poly (Glycerol sebacate) materials: an antimicrobial material for wound dressing, Polymers 12 (7) (2020).
[28] T. Murray Stewart, T.T. Dunston, P.M. Woster, R.A. Casero Jr., Polyamine catabolism and oxidative damage, J. Biol. Chem. 293 (48) (2018) 18736–18745.
[29] K.Y. Lee, D.J. Mooney, Alginate: properties and biomedical applications, Prog. Polym. Sci. 37 (1) (2012) 106–126.
[30] S. Shen, X. Chen, Z. Shen, H. Chen, Marine polysaccharides for wound dressings application: an overview, Pharmaceutics 13 (10) (2021).
[31] C.A. McBride, R.M. Kimble, K. Stockton, Three donor site dressings in pediatric split-thickness skin grafts: study protocol for a randomised controlled trial, Trials 16 (2015) 43.
[32] J. Li, J. He, Y. Huang, Role of alginate in antibacterial finishing of textiles, Int. J. Biol. Macromol. 94 (Pt A) (2017) 466–473.
[33] K. Varaprasad, T. Jayaramudu, V. Kanikireddy, C. Toro, E.R. Sadiku, Alginate-based composite materials for wound dressing application:A mini review, Carbohydr. Polym. 236 (2020), 116025.
[34] S. Liu, T. Jiang, R. Guo, C. Li, C. Lu, G. Yang, J. Nie, F. Wang, X. Yang, Z. Chen, Injectable and degradable PEG hydrogel with antibacterial performance for promoting wound healing, ACS Appl. Bio Mater. 4 (3) (2021) 2769–2780.
[35] D.M. Knapp, V.H. Barocas, A.G. Moon, K. Yoo, L.R. Petzold, R.T. Tranquillo, Rheology of reconstituted type I collagen gel in confined compression, J. Rheol. 41 (5) (1997) 971–993.
[36] J. Lee, E. Ban, H. Park, A. Kim, Stability enhancement of freeze-dried Gelatin/alginate coacervates for bFGF delivery, Pharmaceutics 14 (12) (2022).
[37] J.L. Webber, N.L. Benbow, M. Krasowska, D.A. Beattie, Formation and enzymatic degradation of poly-l-arginine/fucoidan multilayer films, Colloids Surf. B Biointerfaces 159 (2017) 468–476.
[38] Q. Xiao, X. Gu, S. Tan, Drying process of sodium alginate films studied by two-dimensional correlation ATR-FTIR spectroscopy, Food Chem. 164 (2014) 179–184.
[39] Z. Krpetić, G. Scarì, E. Caneva, G. Speranza, F. Porta, Gold nanoparticles prepared using cape aloe active components, Langmuir 25 (13) (2009) 7217–7221.
[40] C. Yu, X. Ying, M.A. Shahbazi, L. Yang, Z. Ma, L. Ye, W. Yang, R. Sun, T. Gu, R. Tang, S. Fan, S. Yao, A nano-conductive osteogenic hydrogel to locally promote calcium influx for electro-inspired bone defect regeneration, Biomaterials 301 (2023), 122266.
[41] R. Rajesh, Y.D. Ravichandran, Development of a new carbon nanotube-alginate-hydroxyapatite tricomponent composite scaffold for application in bone tissue engineering, Int. J. Nanomed. 10 (Suppl 1) (2015) 7–15. Suppl 1.
[42] R. Wang, Y. Ma, S. Zhan, G. Zhang, L. Cao, X. Zhang, T. Shi, W. Chen, B7-H3 promotes colorectal cancer angiogenesis through activating the NF-κB pathway to induce VEGFA expression, Cell Death Dis. 11 (1) (2020) 55.
[43] M. Malone, G. Schultz, Challenges in the diagnosis and management of wound infection, Br. J. Dermatol. 187 (2) (2022) 159–166.
[44] F. Saporito, G. Sandri, M.C. Bonferoni, S. Rossi, C. Boselli, A. Icaro Cornaglia, B. Mannucci, P. Grisoli, B. Vigani, F. Ferrari, Essential oil-loaded lipid nanoparticles for wound healing, Int. J. Nanomed. 13 (2018) 175–186.
[45] P. Wang, Y. Pu, Y. Ren, S. Liu, R. Yang, X. Tan, W. Zhang, T. Shi, S. Li, B. Chi, Bio-inspired hydrogel-based bandage with robust adhesive and antibacterial abilities for skin closure, Sci. China Mater. 65 (1) (2022) 246–254.
[46] C.H. Lim, Q. Sun, K. Ratti, S.H. Lee, Y. Zheng, M. Takeo, W. Lee, P. Rabbani, M. V. Plikus, J.E. Cain, D.H. Wang, D.N. Watkins, S. Millar, M.M. Taketo, P. Myung, G. Cotsarelis, M. Ito, Hedgehog stimulates hair follicle neogenesis by creating inductive dermis during murine skin wound healing, Nat. Commun. 9 (1) (2018) 4903.
[47] Z.I. Elbialy, D.H. Assar, A. Abdelnaby, S.A. Asa, E.Y. Abdelhiee, S.S. Ibrahim, M. M. Abdel-Daim, R. Almeer, A. Atiba, Healing potential of Spirulina platensis for skin wounds by modulating bFGF, VEGF, TGF-ß1 and α-SMA genes expression targeting angiogenesis and scar tissue formation in the rat model, Biomed. Pharmacother. 137 (2021), 111349.
[48] P. Ebner-Peking, L. Krisch, M. Wolf, S. Hochmann, A. Hoog, B. Vári, K. Muigg, R. Poupardin, C. Scharler, S. Schmidhuber, E. Russe, H. Stachelscheid, A. Schneeberger, K. Schallmoser, D. Strunk, Self-assembly of differentiated progenitor cells facilitates spheroid human skin organoid formation and planar skin regeneration, Theranostics 11 (17) (2021) 8430–8447.
[49] D. Nanba, F. Toki, K. Asakawa, H. Matsumura, K. Shiraishi, K. Sayama, K. Matsuzaki, H. Toki, E.K. Nishimura, EGFR-mediated epidermal stem cell motility drives skin regeneration through COL17A1 proteolysis, J. Cell Biol. 220 (11) (2021).
[50] Y. Ding, P. Yang, S. Li, H. Zhang, X. Ding, Q. Tan, Resveratrol accelerates wound healing by inducing M2 macrophage polarisation in diabetic mice, Pharm. Biol. 60 (1) (2022) 2328–2337.
[51] H. Lee, W. Chun, G. Kim, Three-Dimensional Artificial skin construct Bioprinted with a Marine-based Biocomposite, Biomacromolecules 24 (6) (2023) 2864–2878.
[52] Y. Zhang, S. Wang, Y. Yang, S. Zhao, J. You, J. Wang, J. Cai, H. Wang, J. Wang, W. Zhang, J. Yu, C. Han, Y. Zhang, Z. Gu, Scarless wound healing programmed by core-shell microneedles, Nat. Commun. 14 (1) (2023) 3431.
[53] H. Nosrati, R. Aramideh Khouy, A. Nosrati, M. Khodaei, M. Banitalebi-Dehkordi, K. Ashrafi-Dehkordi, S. Sanami, Z. Alizadeh, Nanocomposite scaffolds for accelerating chronic wound healing by enhancing angiogenesis, J. Nanobiotechnol. 19 (1) (2021) 1.
[54] G. Soong, F.J. Martin, J. Chun, T.S. Cohen, D.S. Ahn, A. Prince, Staphylococcus aureus protein A mediates invasion across airway epithelial cells through activation of RhoA GTPase signaling and proteolytic activity, J. Biol. Chem. 286 (41) (2011) 35891–35898.
[55] C.G. Wang, Y.T. Lou, M.J. Tong, L.L. Zhang, Z.J. Zhang, Y.Z. Feng, S. Li, H.Z. Xu, C. Mao, Asperosaponin VI promotes angiogenesis and accelerates wound healing in rats via up-regulating HIF-1α/VEGF signaling, Acta Pharmacol. Sin. 39 (3) (2018) 393–404.